Michael Maas, Carolina C. Silvério, Jens Laube, Kurosch Rezwan

Electrostatic assembly of zwitterionic and amphiphilic supraparticles

Journal Article as: peer-reviewed accepted version (Postprint)

DOI of this document*(secondary publication): 10.26092/elib/2614

Publication date of this document: 25/10/2023

* for better findability or for reliable citation

Recommended Citation (primary publication/Version of Record) incl. DOI:

Michael Maas, Carolina C. Silvério, Jens Laube, Kurosch Rezwan,
Electrostatic assembly of zwitterionic and amphiphilic supraparticles,
Journal of Colloid and Interface Science, Volume 501, 2017, Pages 256-266, ISSN 0021-9797,
https://doi.org/10.1016/j.jcis.2017.04.076

Regular Article

Electrostatic assembly of zwitterionic and amphiphilic supraparticles

Michael Maas [a,c,*], Carolina C. Silvério [a], Jens Laube [b,c], Kurosch Rezwan [a,c]

[a] Advanced Ceramics, University of Bremen, Bremen, Germany
[b] Hybrid Materials Interfaces Group, University of Bremen, Bremen, Germany
[c] MAPEX Center for Materials and Processes, University of Bremen, Bremen, Germany

GRAPHICAL ABSTRACT

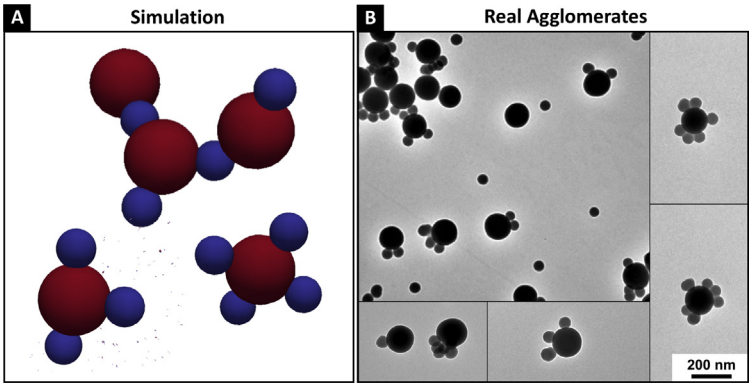

Keywords:
Supraparticles
Patchy particles
Electrostatic heteroaggregation
Pickering emulsion
DLVO
Silica
Simulation

ABSTRACT

We demonstrate the electrostatic assembly of oppositely charged silica particles into an ensemble of well-defined core-satellite supraparticles, which are a type of patchy particle. To achieve controlled heteroaggregation, we used oppositely charged silica particles with different sizes ranging from 5 nm to 150 nm at several concentrations. The assembly works best with larger particles, resulting in a fairly low polydispersity and a low amount of bridging between the individual clusters. Using smaller particles produces high polydispersity, large clusters and uncontrolled aggregation and bridging. Furthermore, even with controlled aggregation into well-defined clusters in the case of bigger particles, we observe an uneven covering of the central particles with around 1–6 satellite particles adsorbed to the central particle. This behavior is not predicted by simple pairwise DLVO potentials which would anticipate an even spacing of the satellite particles on the core. We explain these observations by taking into account the interactions of the adsorbing particles within the ionic cloud of the central particle. We hypothesize that when the adsorbing satellite particles are small compared to the diameter of the ion cloud of the core particle, they aggregate within the ion cloud and therefore do not create a well-defined monolayer on the surface of the core particle, instead forming small agglomerates during adsorption.

Finally, both the assembled zwitterionic clusters and clusters that were partially hydrophobized were tested for their capabilities as Pickering emulsifiers. The zwitterionic clusters showed a strongly increased surface activity compared to the individual particles, while the hydrophobized particles changed the emulsion type from w/o to o/w. Interfacial dilatational rheological tests supported the

* Corresponding author at: University of Bremen, Advanced Ceramics, Am Biologischen Garten 2, 28359 Bremen, Germany.
E-mail address: michael.maas@uni-bremen.de (M. Maas).

observations from the emulsion tests. With this, we demonstrate that a relatively unordered ensemble of supraparticles is able to show well-defined functionality at a higher hierarchical level as Pickering emulsifiers.

1. Introduction

The colloidal assembly of individually dispersed nanoparticles into well-defined clusters consisting of only a few nanoparticles promises the scalable synthesis of advanced multifunctional supraparticles with well-defined surface moieties, also known as patchy particles. A facile and scalable synthesis route of patchy supraparticles would enable the fabrication of complex and functional colloidal assemblies, giving rise to non-hexagonal colloidal crystals [1], tailorable metamaterials [2] and eventually to complex nanomachines [3]. However, electrostatic heteroaggregation, which uses oppositely charged particles, and which is one of the simplest approaches to colloidal assembly, usually results in the uncontrolled precipitation of large clusters of particles. This general observation is opposed to a number of computational studies which predict that the controlled assembly of patchy particles via electrostatic assembly should be possible [4,5].

Next to the above mentioned visionary applications for particles that feature directional bonding, controlled surface anisotropy of heteroaggregate particles could give rise to particles with increased surface activity due to intermediate wetting properties of the particle surface, which should lead to an improved ability to stabilize Pickering emulsions [6,7]. In this respect, nanoscale heteroaggregates are reminiscent of the complex charge distribution in proteins, especially on the surfaces of virus capsids [8]. Hence, nanoparticles with localized surface regions of varying charge (or further properties like hydrophilicity) could prove to be a powerful addition to the portfolio of biofunctional colloids [9].

The term heteroaggregation is used to describe the instability of colloidal dispersions that consist of more than one type of particle [10]. The particles may differ in a variety of properties, including composition, shape, size, surface potential and charge. Here, we only address electrostatic heteroaggregation, i.e. the aggregation between oppositely charged nanoparticles as a result of Coulomb interactions. Heteroaggregates can be stable or unstable, depending on whether the aggregates remain as regular and well-dispersed units or whether they exist in large irregular masses that will eventually precipitate [5,12]. This behavior is also dependent on the relative particle sizes: particles similar in size tend to form large percolating agglomerates, giving rise to irregular clusters of particles. If there is a large difference in particle size, the smaller particles may adsorb onto the surface of the larger species creating a cohesive surface coating of the smaller particles on a central template particle [11,13,14]. Additionally, particle concentrations [15], surface functionalization [16] and solvent composition [17] also play a role in determining the final outcome of the aggregation process.

The interactions between colloidal particles with identical properties, called homoaggregation, can be appropriated by the DLVO theory [18]. The central assumption of the DLVO theory is the separation of the total interaction potential between two particles into attractive and repulsive contributions:

$$V_{DLVO} = V_A + V_R \tag{1}$$

The repulsive interactions are usually electrostatic in nature and arise due to the electrical double layer surrounding the spheres, originating from ionizable groups on the particle surface. When the particles are the same, the resultant force is repulsive; when the particles differ in charge, as in heteroaggregation, the electrostatic forces are attractive. The electrical double layer can be quantified by the Debye-Hückel theory. It describes the thickness of the ion cloud surrounding a particle with the characteristic Debye-Hückel length κ^{-1} which is the distance from the particle surface at which the surface potential is merely 1/e of its initial value.

The electrostatic surface potential ψ of a particle with radius a as a function of the distance r from its surface can be approximated as

$$\psi(r) = \psi_0 \frac{a}{r} \exp(-\kappa(r-a)) \tag{2}$$

with the Debye-Hückel length κ^{-1} defined as

$$\kappa^{-1} = \sqrt{\frac{\varepsilon \cdot k_B \cdot T}{2 \cdot N_A \cdot e^2 \cdot I}} \tag{3}$$

Based on the Poisson-Boltzmann equation, the gradient of the ion concentration c in the ionic cloud can be written as

$$c = c_0 \cdot \exp\left(\frac{e\psi(r)}{k_B T}\right) \tag{4}$$

where c_0 is the ion concentration in the bulk phase and e is the elementary charge [19,20].

The attractive forces between colloidal particles usually consist of van der Waals forces which are a result of temporary dipoles and depend on the Hamaker constant A and the particle geometry. When expressed in terms of interaction energy, the DLVO potential can be written as

$$W_{DLVO} = W_{vdW} + V_{Coulomb} \tag{5}$$

with

$$W_{vdW}(r) = -A\frac{a}{12r} \tag{6}$$

and

$$W_{Coulomb}(r) = \frac{64\pi \cdot k_b T \cdot a \cdot I \cdot \gamma^2}{\kappa^2} e^{-\kappa r} \tag{7}$$

with $\gamma = \tanh(\Psi/4)$, $\Psi = ve\psi/kT$, the ionic strength I, the Boltzmann constant k_b and the temperature T [21].

However, the DLVO theory only provides a basic framework to assess particle interactions in real-life systems. It has especially limited accuracy for systems with high ionic strength, submicron particles and interactions with more than two particles at one time.

There are a few notable exceptions to the otherwise suspicious lack of publications on stable heteroaggregates. For example, Dušak et al. studied the adsorption of small carboxylated maghemite nanoparticles to amino-functionalized silica particles and found that electrostatic heteroaggregation results in an uneven coating on the silica particles while covalent attachment gave rise to fairly well-defined structures [22]. Wagner et al. achieved a very regular coating of aminated polystyrene particles 154 nm in diameter with negatively charged gold or magnetite particles with diameters around 20 nm. Here, all particles showed notably high zeta-potentials above ±70 mV which might explain the even spacing of the smaller particles on the bigger ones [23]. Alternative

strategies of supraparticle synthesis like the assembly inside emulsion droplets or coordinating particles via DNA recognition have been more successful for creating well-defined supraparticles. See [24–26] for comprehensive reviews on alternative strategies for the synthesis of patchy supraparticles.

In this work, we are using silica colloids with tailored surface chemistry as a well-defined system to study the formation of stable heteroaggregates with a range of particle sizes. Our goal was to create colloidally stable supraparticles consisting of a positively charged nanoparticle at the center, to which a limited number of smaller, negatively charged particles are attached. We discuss our findings in light of our own simulations as well as on a calculation of the DLVO interactions which lead to cluster formation of small particles on bigger particles. Finally, we investigate whether the supraparticles show improved surface activity as Pickering emulsifiers. To this end, we also created amphiphilic particles which build on the previously assembled zwitterionic supraparticles by specifically hydrophobizing only the negatively charged regions of the supraparticle surface.

2. Materials and methods

2.1. Materials

(3-Aminopropyl)triethoxysilane (APTES) (purity >99%), decane (anhydrous purity ≥99%) and Ludox TMA colloidal silica (34 wt%) were purchased from Sigma Aldrich (Munich, Germany). Octadecyltrimethoxysilane (OTMS) (purity >97%) was obtained from abcr (Karlsruhe, Germany). The silica particles with nominal sizes of 150 nm and 80 nm were purchased from Fiber Optic Center (New Bedford, MA, USA. Detonation Nanodiamonds (G01) were purchased from Plasmachem (Berlin, Germany). The experiments were performed using double deionized water with a conductivity of 0.04 μS cm^{-1} from a Synergy apparatus (Merck Millipore, Darmstadt, Germany) which was adjusted to pH 5 by setting a NaOH concentration of 10^{-5} mol/L.

Table 1
Concentration of 80 nm particles in g/ml and the weight ratio between the APTES coated 150 nm particles (A150) and 80 nm silica particles.

Concentration of 80 nm particles (mg/ml)	Weight ratio of A150:80	Number ratio of A150:80
0.8	1:0.16	1:1
2	1:0.4	1:2.6
5	1:1	1:6.6

2.2. APTES functionalization

The 150 nm silica particles were functionalized with (3-aminopropyl)triethoxysilane (APTES) in order to change their surface charge from negative to positive at pH 5. The particles were dissolved in toluene (0.05 g/ml) using an ultrasonic bath. Using a Schlenk set-up the dispersion was heated to 110 °C. 21 μl of APTES for each 1 ml of solvent was added and the system was left under medium stirring for six hours, while a flux of nitrogen gas was supplied for the first 20 min. After six hours, the particles were washed twice in ethanol and once in Millipore water with alternating centrifugation/redispersion cycles. Finally, the particles were dried in a drying cabinet at 70 °C for 24 h, resulting in positively charged 150 nm silica particles (labeled A150).

2.3. Electrostatic self-assembly

The positively charged A150 particles were dispersed in Millipore water at pH 5. A separate dispersion was prepared under the same conditions for the negatively charged silica particles with a diameter of 80 nm (in the following denoted as 80). Then, the two dispersions were mixed and immediately agitated with the help of a vortex for about 30 s. Afterwards the dispersions were centrifuged at low speed (200 rpm) for 2 min to reduce bigger aggregates. Three mixing ratios of A150:80 were studied. The concentration of the A150 particles was fixed at 5 mg/ml and the concentration of 80 nm particles varied according to Table 1.

Additionally, the heteroaggregation was examined using different particle sizes. The combination of particle sizes investigated are summarized in Table 2. With the exception of the 5 nm sized nanodiamonds, silica particles were used for all experiments. The bigger particles were coated with APTES as described above. The concentration of the bigger particles was fixed at 5 mg/ml, for the concentration of the smaller particles we tested 0.005 mg/ml, 0.5 mg/mL and 2 mg/ml. Only concentrations of 0.5 mg/ml will be shown, since the experiments with higher and lower small particles concentrations revealed no additional information.

2.4. OTMS functionalization

For the emulsions studies, a portion of the assembled particles (A150+80) were coated using octadecyltrimethoxysilane (OTMS) which has a hydrophobic octadecyl hydrocarbon chain that renders the particle surface hydrophobic. The negatively charged 80 nm particles are coated preferentially due to the already present APTES coating on the 150 nm particles resulting in amphiphilic

Table 2
Overview over particle functionalizations and assemblies.

	Functionalization	Zeta potential at pH 5	Abbreviation
Single particles			
Silica, 150 nm	None	−35.5 ± 0.3 mV	150
Silica, 80 nm	None	−31.9 ± 0.6 mV	80
Silica, 150 nm	APTES	+31.1 ± 0.8 mV	A150
Silica, 150 nm	OTMS	/[a]	150+OTMS
Silica, 150 nm	OTMS	/[a]	80+OTMS
Silica, 150 nm	APTES and OTMS	/[a]	A150+OTMS
Silica, 25 nm	None	−35.7 ± 0.7 mV	
Nanodiamond	Annealed in air	−42 ± 2.9 mV	ND-
Assembled particles			
Silica, 150 nm/Silica, 80 nm	APTES/none	−2.7 ± 1.1 mV	A150+80
Silica, 150 nm/Silica, 80 nm	APTES/none and OTMS	/[a]	A150+80+OTMS
Silica, 80 nm/ND, 5 nm	APTES/none	/[a]	A80+ND
Silica, 80 nm/Silica, 30 nm	APTES/none	/[a]	A80+30
Silica, 150 nm/Silica, 30 nm	APTES/none	/[a]	A150+30

[a] Unstable dispersions in water.

nanoparticles. 1 g of the supraparticles were dispersed in 100 ml of ethanol followed by the addition of 1 ml of ammonia (25%). The solution was left with vigorous stirring at room temperature for 10 min. Then, 10 ml of an OTMS solution in chloroform (10 w%) was added dropwise into the reaction mixture. The reaction was left stirring for 24 h. Afterwards, the particles were separated and washed three times with ethanol using alternating centrifugation/redispersion cycles. The amphiphilicity of the particles was confirmed using the heptane absorption method (see supplementary information).

2.5. Emulsification test

Particle suspensions were prepared with a concentration of 1 mg/ml in 20 ml water or in decane for the particles treated with OTMS. After that, the same volume of either decane or water was added to the particle suspension. All samples were hand shaken for about 30 s at the same time to create emulsions. The following samples were prepared: bare 80 nm silica particles (80), 80 nm silica particles functionalized with OTMS (80+OTMS), bare 150 nm silica particles (150), 150 nm silica particles functionalized with OTMS (150+OTMS), 150 nm silica particles functionalized with APTES (A150), A150 functionalized additionally with OTMS (A150 +OTMS), the assembled A150 particles with 80 nm particles (A150+80) and A150+80 nm functionalized with OTMS (A150+80 +OTMS). In order to monitor the emulsion stability, pictures of the emulsions were taken before the shaking step (0) and 1, 5, 15, 30 and 60 min after shaking.

2.6. Pendant drop interfacial dilatational rheology

To determine the interfacial dilatational rheology of the emulsion droplets, a pendant drop tensiometer equipped with a needle of 0.5 mm diameter (OCA25 from Dataphysics, Germany) was used. The setup and the methodology is described elsewhere [27].

For the rheological tests, a 6 μL drop of water in a surrounding decane phase was analyzed. The hydrophilic particles were dispersed in the water phase and the OTMS-functionalized particles in the decane phase at a concentration of 10 mg/ml. The same particle combinations were tested as in the emulsion experiments. After determining the linear viscoelastic range at an oscillation frequency of 0.5 Hz, time tests were performed at a constant frequency of 0.5 Hz and a deformation amplitude of 5% dV/V for one hour.

2.7. Particle characterization

Particle morphologies were visualized by transmission electron microscopy (TEM, Oxford Instruments – JEOL JEM 2011 and Zeiss – EM 900) and scanning electron microscopy (SEM, Zeiss – Supra 40). For sample preparation, the dispersions were diluted with isopropanol at a volume ratio of 1:1 to reduce aggregation during drying. For SEM, a droplet of the dispersion was placed on a silicon wafer or copper grid and dried at 70 °C for 2 h. For TEM, a droplet of the dispersion was placed on a copper grid with Formvar film and dried in air. The samples did not require staining or sputtering.

The size and zeta potential were determined using a Zetasizer Nano ZSP (Malvern Instruments). The data are given as mean ± standard deviation based on three independent measurements.

2.8. Modeling

To investigate the detailed agglomeration mechanisms inside the suspensions, Brownian dynamics simulations were performed on different initially undisturbed suspension models. These models were generated by repeatedly placing particles at equal distances to each other into a periodic simulation box. Different particle species were placed into different cell regions to mimic a heterogeneous suspension before mixing. The forces acting on the single particles due to the influence of the surrounding solvent were calculated by a Langevin thermostat as described in [4] with a dynamic viscosity of the solvent $\eta = 10^{-3}$ Pa s. The DLVO potential was calculated from the above equations by using a surface potential of +35 mV for the positively charged particles and of −35 mV for the negatively charged particles (which is approximated based on our zeta-potential measurements), a temperature of 293 K, an ion concentration in the solution of 10^{-5} mol/l and a Hamaker constant of $0.46 * 10^{-20}$ J. To prevent the particles from penetrating each other, a repulsive Hookean spring potential was applied at particle contact and rearrangement of the particles after agglomeration was disabled by applying large friction coefficients. The simulations were performed for a duration of 0.5 s by using the LIGGGHTS simulation package [28] with a timestep of 10^{-9} s.

3. Results and discussion

3.1. Characterization of the supraparticles

We begin the discussion of the experimental results with a simple control experiment using unmodified silica particles with diameters of 150 nm and 80 nm (called 150 and 80 in the following) carrying a negative surface charge of −35.5 ± 0.3 mV and −31.9 ± 0.6 mV at pH 5 (see also Table 2). In this case, the particles do not aggregate and form a stable dispersion (Fig. 1a). In contrast, when the central particles are coated with APTES (called A150 in the following), which results in a zeta potential of +31.1 ± 0.8 mV at pH 5, the particles immediately aggregate and form small clusters (Fig. 1b).

3.2. Influence of particle ratio

The nature of the resulting clusters strongly depends on the number ratio between these two types of particles (A150 and 80). While more number ratios were analyzed in preliminary experiments, the ratios 1:6.6. 1:2.6 and 1:1 were chosen for further investigation because they represent the heteroaggregation behavior based around the most stable ratio of 1:2.6. A high ratio of small particles to big particles (1:6.6) results in uncontrolled aggregation and the formation of large clusters (Fig. 2a). This is also evident in the intensity weighted size distribution obtained by dynamic light scattering (Fig. 2a, right) which shows a wide curve with a median value of 513 ± 18 nm and a broad size distribution. Since the absorption of a high number of negatively charged particles onto the bigger, positively charged particles leads to a charge reversal of the resulting supraparticle, we expect that the particles aggregate as soon as the surface charge of the central particles becomes neutralized. Alternatively, in the case of an uneven absorption of small particles, aggregation could take place between supraparticles that still carry a net-positive charge and those that are already negatively charged.

A low number ratio of A150 to 80 particles (1:1) also leads to the formation of unstable heteroaggregates (Fig. 2c) which is most likely caused by the small particles forming bridges that link two A150 particles. However, the uncontrolled agglomeration is less excessive as in the case of a high ratio. The DLS data show a fairly high amount of stable aggregates with a size of around 300 nm next to bigger aggregates.

At a moderate number ratio (1:2.6), the formation of stable heteroaggregates can be achieved (Fig. 2b). Note that the TEM images do not represent the aggregation state, since many aggre-

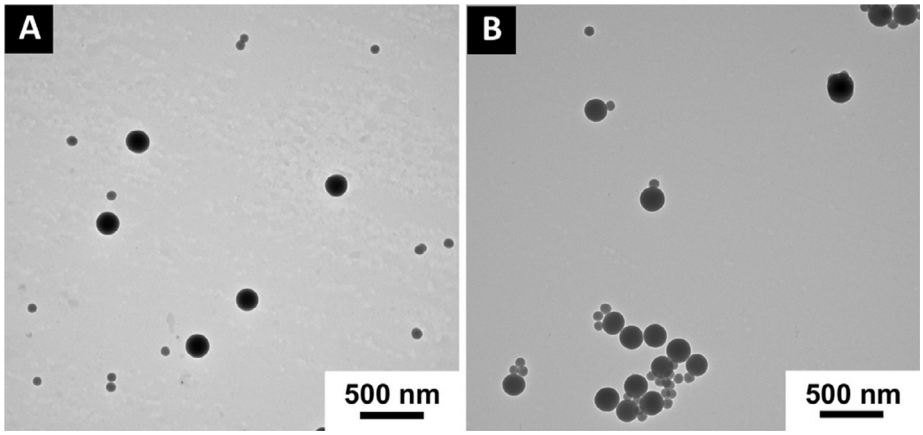

Fig. 1. (A) Control experiment with unmodified silica particles (d = 150 and 80 nm) with identical negative surface charge showing no agglomeration and (B) the bigger particles (d = 150 nm) are coated with APTES resulting in a positive surface charge which leads to heteroagglomeration with the negatively charged 80 nm particles.

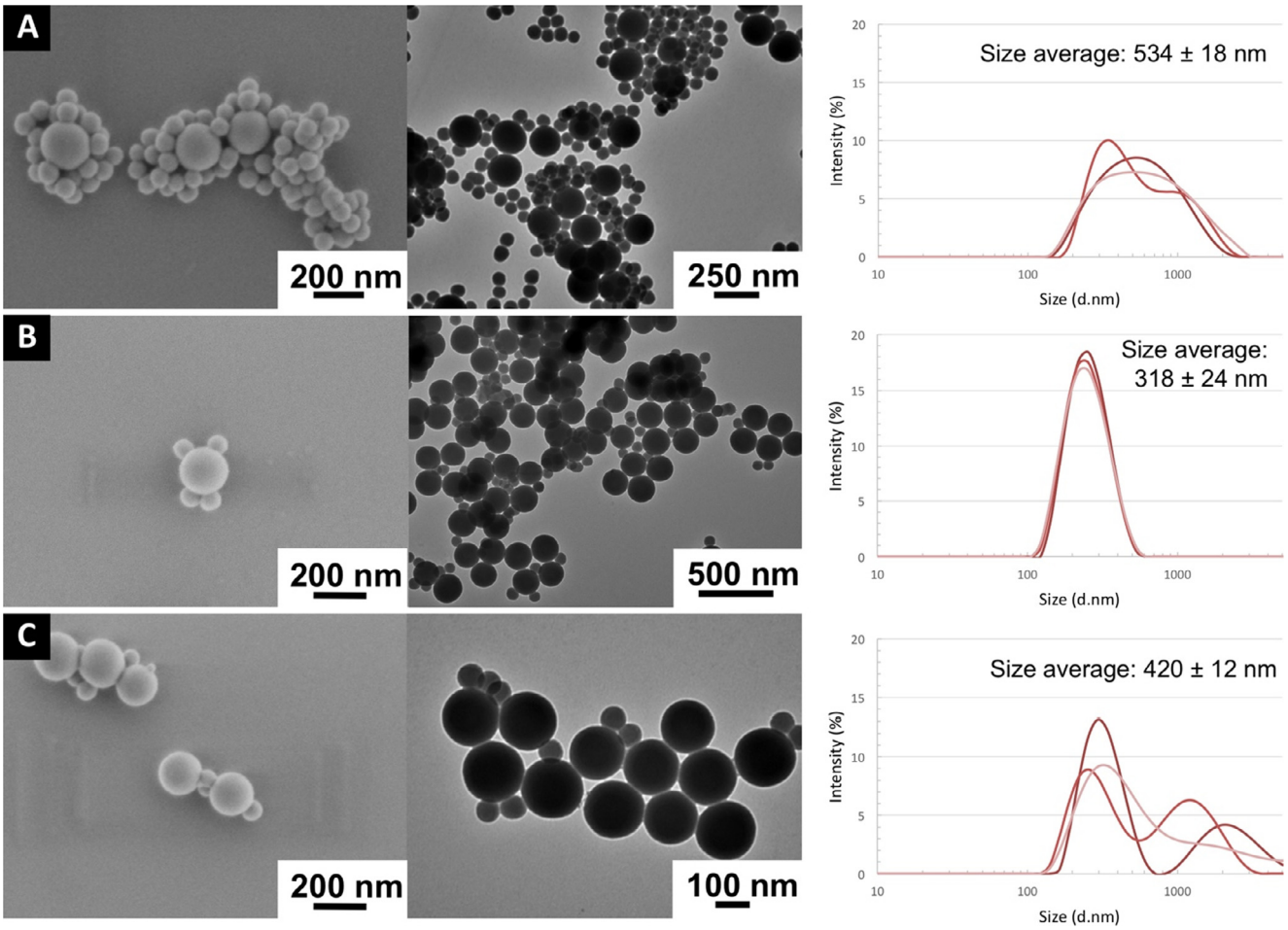

Fig. 2. Variation of the number ratio between positively charged 150 nm and negatively charged 80 nm silica particles. Number ratio big to small particles (A) 1:6.6, (B) 1:2.6, (C) 1:1. Left panel: SEM micrographs, middle panel: TEM micrographs, right panel: intensity weighted size distribution determined by DLS.

gates might have formed during drying. The median hydrodynamic radius of the resulting supraparticles is 318 ± 24 nm, which corresponds very well to a central particle with a diameter of 150 nm plus one or several 80 nm particles extending the radius of gyration (which would correspond to the maximum diameter of a central 150 nm particle plus two 80 nm particles on opposite sites). The intensity weighted DLS results (Fig. 2b, right) show a remarkable absence of bigger aggregates, although the overall zeta potential of the supraparticles is very low (−2.7 ± 1.1 mV). However, we do not observe an evenly distributed number of small particles adsorbed to the bigger particles. Instead, supraparticles consisting of one central A150 particle and one to six 80 nm particles are found (see Fig. 4c for further images of stable supraparticles). Additionally, the particles do not adsorb with an even spacing.

Conversely, the smaller particles seem to aggregate with each other while being adsorbed on the bigger particles. The last observation can also be seen for the unstable clusters (Fig. 2a and c).

3.3. Influence of particle size

The same experiments were performed using combinations of smaller particles. Mixtures of A150 and 25 nm particles (called 25 in the following), APTES coated 80 nm particles (called A80 in the following) and 25, as well as A80 and nanodiamonds (ND) with a diameter of about 5 nm were tested at the same range of number ratios as the A150+80 tests described above. With none of these combinations, stable heteroaggregates could be observed. Instead, all samples showed very high polydispersity that prevented reliable DLS results. Interestingly, the TEM micrographs show that the smaller 25 nm silica particles formed multilayer aggregates on the bigger particles, although the electrostatic repulsion should be considerably high due to a zeta potential of the small particles of -35.7 ± 0.7 nm (Fig. 3a,b). This behavior was even more pronounced with nanodiamonds which exhibit a zeta-potential of -42 ± 2.9 mV. Here, small nanodiamond clusters of around 60 nm were observed absorbing to the A80 particles (Fig. 3c).

3.4. Rationalization of aggregation behavior

The aggregation between small particles that are adsorbed to bigger particles is a phenomenon that is usually not predicted in simulation experiments. If, during adsorption, pairwise DLVO interactions between all particles are maintained in the same way in solution as in vicinity to bigger, oppositely charged particles, then the small particles should repel each other at all times, leading to an even spacing of small particles adsorbed to the oppositely charged central particle as was shown in the dynamic modeling analysis (Fig. 4a). In contrast to the experimental findings, our simulations even find a lower agglomeration tendency for the smaller satellite particles due to the fast occupation of all connection points at the central particles.

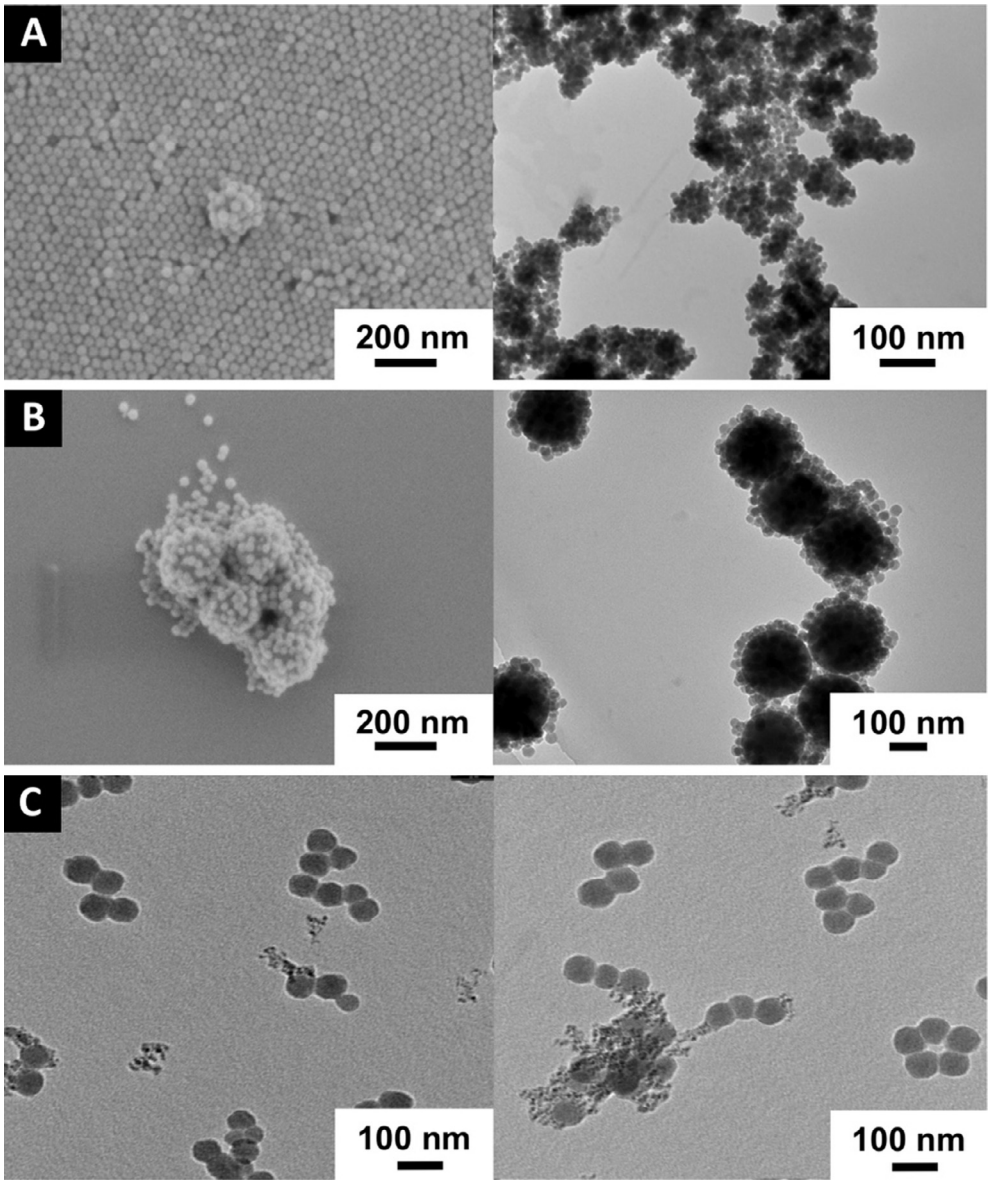

Fig. 3. Using even smaller particles results in uncontrolled agglomeration. Particle diameters (A) APTES coated 80 nm and uncoated 25 nm silica particles, (B) APTES coated 150 nm and uncoated 25 nm silica particles, and (C) APTES coated 80 nm silica and negatively charged 5 nm nanodiamond particles.

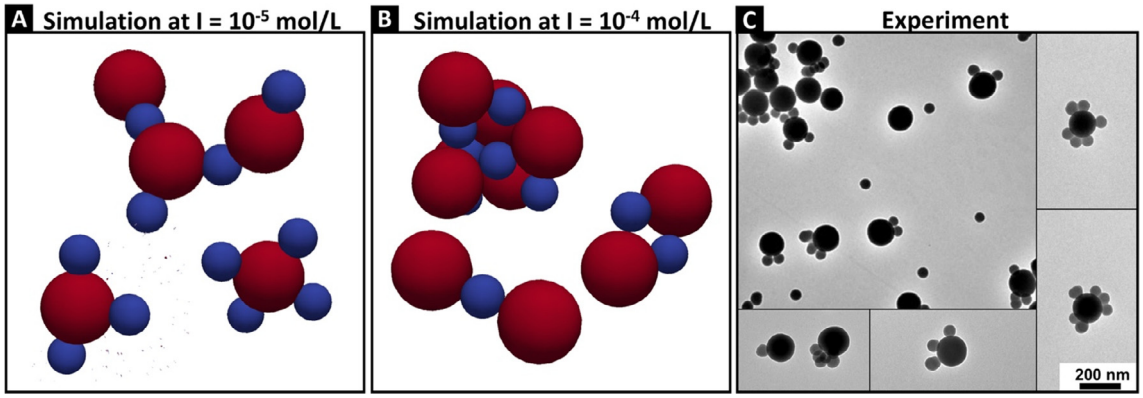

Fig. 4. (A) Based on simulated pairwise DLVO interactions, the small particles should have minimum distances on the surface of the big particle based on Coulomb repulsion, overall ionic strength $I = 10^{-5}$ mol/L. (B) as (A), but with an ionic strength of $I = 10^{-4}$ mol/L between the smaller particles. (C) Collage of TEM images of zwitterionic supraparticles at a number ratio of 1:2.6 (see Fig. 2b), scale bar applies to all subimages.

Instead of the even spacing of small nanoparticles as predicted by our modeling experiment, we observe an uneven coating and aggregation of small particles adsorbed to the central particle (Fig. 4c). A simple explanation for this phenomenon would be that the adsorption of small particles to the oppositely charged bigger particles is governed by kinetics, or in other words, that the particles stay at the position that they first adsorb without being able to equilibrate into thermodynamically favored distances. However, although our simulation does not allow for a rearrangement of the particles once they are adsorbed, the small particles are able to equilibrate their distances on account of the pair-wise interactions between each particle during the adsorption process. Accordingly, the kinetic approach does not seem to explain the observed aggregation behavior.

Not modeled so far in our simulation is the change of interactions between small particles during their approach towards the bigger particle (Fig. 5). However, the influence of the ionic cloud of the central particle on the colloidal stability of the small particles might be significant. At pH 5 the Debye-Hückel length of the ionic cloud of an A150 particle is roughly 100 nm (Fig. 6a). Inside the ion cloud, the ion concentration is up to 4 times higher than in the bulk phase (Fig. 6b). This increase in ionic strength needs to be factored in when considering the DLVO interactions between the smaller particles in close proximity to the bigger particle. Fig. 6c shows a calculation of the DLVO interactions between two 150 nm particles with zeta potentials of 35 mV at pH 5 which corresponds to an ionic strength of 10^{-5} mol/L based on Eqs. (5)–(7) and using a Hamaker constant for silica of $4.6 \cdot 10^{-21}$ J [12,29,30]. The combined curve obtained from the addition of van der Waals attraction and Coulomb repulsion represents a very stable dispersion with repulsive Coulomb interactions in the order of over one hundred k_BT. The combined potential between two 80 nm particles in the bulk phase also shows a stable dispersion, albeit with repulsive potential that is only half as high. When factoring in the increased ionic strength that the 80 nm particles experience in close proximity to the bigger particles, the repulsive interactions are again strongly reduced. Although in our calculations the repulsive interactions inside the ion cloud of the central particle still dominate, the overall reduction of the potential might indicate that the small particles could aggregate during their approach to the central particle. This trend can be extended to even smaller particles in which case the potentials would be further reduced. Furthermore, the diameter of the ion cloud is only to a small degree dependent on the particle size if the surface potential is comparable (±35 mV in our calculations, Fig. 6a and b). Hence, with smaller particle sizes, the influence of ion cloud interactions during the

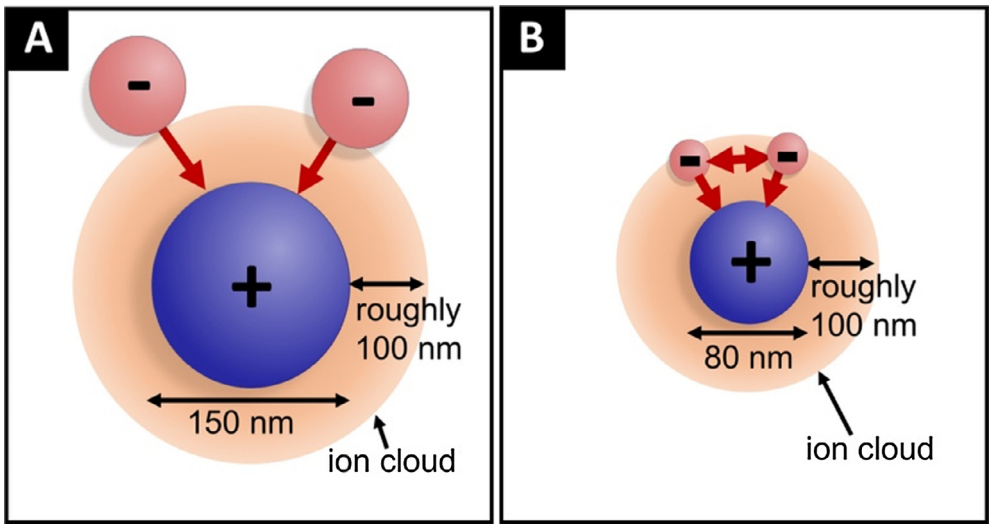

Fig. 5. The ratio of the diameter of the electrostatic cloud around the center particle in relation to the size of the adsorbing particles determines the repulsive/attractive interaction between the adsorbing particles.

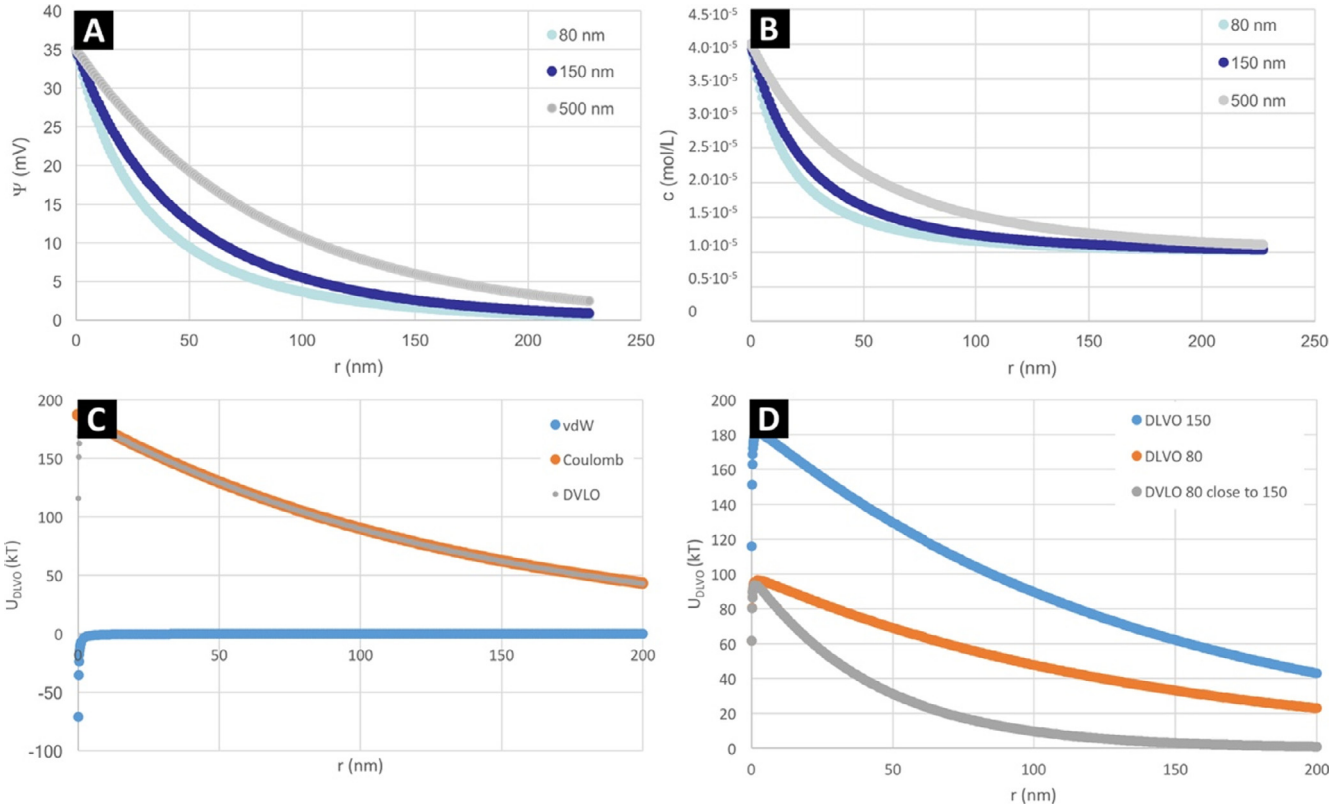

Fig. 6. (A) Electrostatic potential as a function of distance from the particle surface, calculated via Eq. (2), (B) and the resulting increase in ion concentration for different particle sizes, calculated via Eq. (4). (C) DLVO potentials (vdW, Coulomb and combined) for 150 nm particles and (D) combined potentials for different particle sizes and 80 nm particles close to the surface of 150 nm particles, calculated via Eqs. (5)–(7).

studied heteroaggregation processes become increasingly more important (Fig. 5b), which might explain the observed lack of stable heteroaggregates with smaller particles (Fig. 3). Indeed, applying in the simulations a tenfold increased ionic strength of 10^{-4} mol/L solely between the satellite particles results in strong agglomeration of the particles and in the formation of a dense covering of the central particles with satellite particles similar to the observations in the experiments (Fig. 4b). Of course, this first assessment of DLVO interactions only describes a general trend of the interaction potentials and more aspects like steric interactions of the gel-like silica surface, hydration of the hydrophilic particles or even depletion interactions in the binary particle mixture need to be taken into account for a quantitative description of this colloidal system. Additionally, we cannot exclude the occurrence of capillary forces that act on the adsorbed particles during drying of the samples during TEM preparation. Capillary forces could arise in a thinning, evaporating water film between adsorbed particles, which would pull the particles together [31]. These capillary forces can also act on very small particles and can be stronger than van der Waals interactions between the agglomerated particles [32]. However, from our theoretical considerations [32–34], we find that the range of capillary forces between hydrophilic particles with a diameter of 80 nm or below is at maximum 3 nm. The height of these capillary forces would be in the range of 1–5 nN for slightly rough particles. As both the range and the height of these potential capillary forces are thus at least one order of magnitude below the interparticle distances between the agglomerated satellite particles and adhesion forces to the large central particle, we conclude that capillary forces can play a role only in very rare cases. Additionally, capillary interactions are not able to predict multilayer formation of small particles on the central particles, as was observed by us, too (Figs. 2 and 3).

3.5. Utilization of the supraparticles as pickering emulsifiers

Finally, we tested the assembled supraparticles (A150+80) for their ability to stabilize emulsions. To this end, a portion of the assembled particles was partially hydrophobized using OTMS (these supraparticles are denoted as A150+80+OTMS). Since the central particle of the supraparticles was already treated with APTES, OTMS functionalization occurred preferentially on the bare silica surfaces of the 80 nm particles giving rise to amphiphilic particles (Supporting Fig. 1). A range of additional dispersions for control experiments were prepared as well, containing the individual particles (80, 150, A150) as well as their OTMS-functionalized pendants (80+OTMS, 150+OTMS, A150 +OTMS). The hydrophilic particles were dispersed in water, while the hydrophobic particles were dispersed in decane. The opposite liquid phase was added and all mixtures were shaken at the same time. First, it can be immediately observed that the hydrophilic particles give rise to water-in-oil emulsions, while hydrophobic and amphiphilic particles stabilize oil-in-water emulsions (Fig. 7). Second, emulsion stability varies greatly with nanoparticle type. The zwitterionic supraparticles (A150+80) clearly show the best ability to stabilize emulsions in this experiment, as basically no coalescence is observed 1 h after shaking. SEM images of the stabilized emulsion droplets reveal that the supraparticles form a cohesive layer on the droplet surface reminiscent of a colloidosome [35], which indicates that the zwitterionic supraparticles are able to form interlocking aggregates at the droplet interface (Supporting Fig. 2). The hydrophobized 150 nm silica particles are all able to stabilize the emulsions, although the assembled particles (A150+80+OTMS) show the least amount of stabilization. In this case emulsion stabilization seems to benefit from the higher hydrophobicity of the individ-

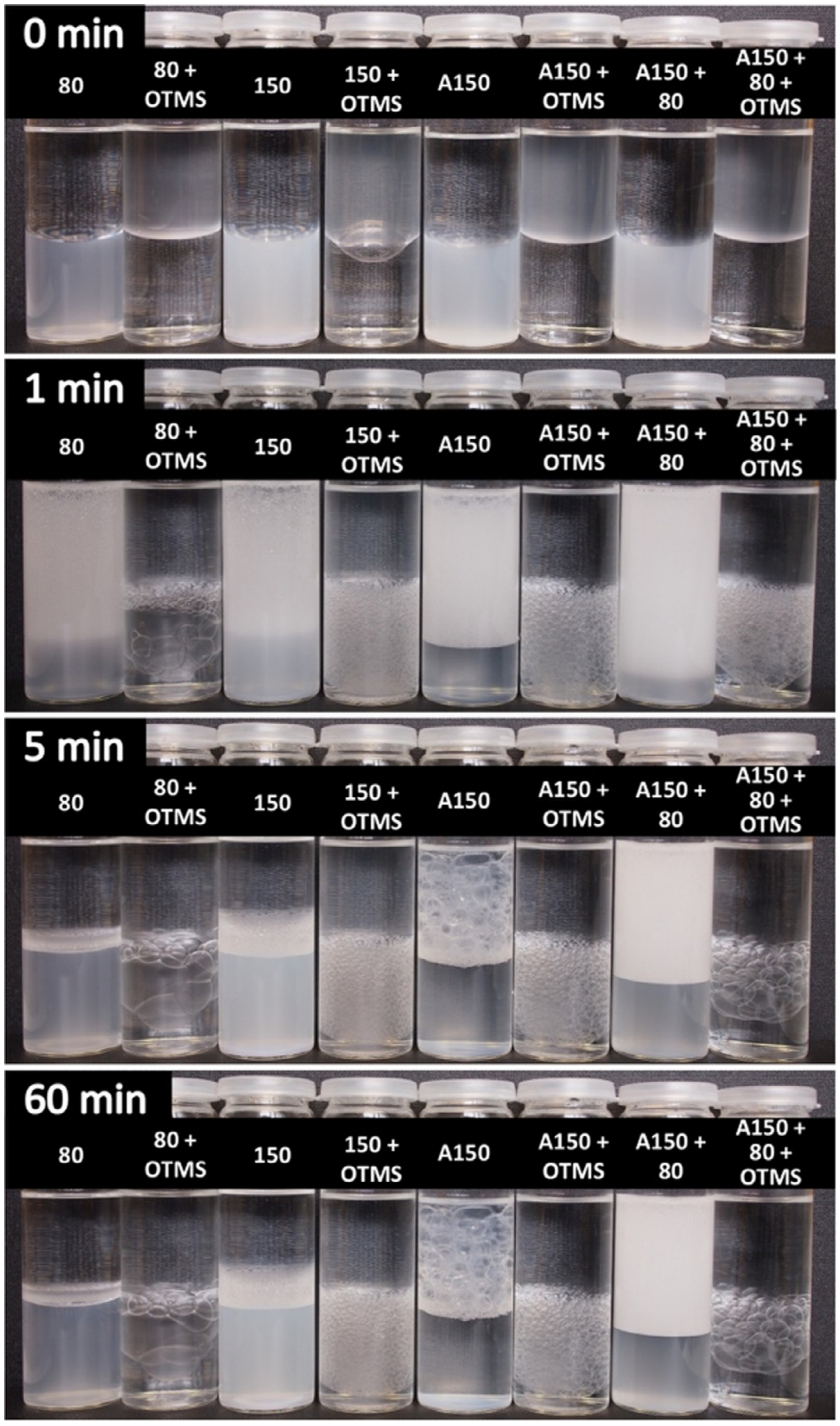

Fig. 7. Pickering emulsions of water and decane using different particles as a function of time after emulsification (0 min: right before shaking). The zwitterionic supraparticles show the best ability to stabilize emulsions. The emulsions are reversed when hydrophobic or amphiphilic particles are used. However, purely hydrophobic particles are better Pickering emulsifiers than the amphiphilic supraparticles.

ual OTMS-coated particles. Since the stabilization of Pickering emulsions is a function of the radius r based on the well-known formula

$$\Delta E = \pi r^2 \gamma (1 - |\cos\theta|)^2 \tag{8}$$

with the stabilization energy ΔE, the interfacial tension γ and the contact angle Θ, the smaller 80 nm particles stabilize the emulsion to a lesser extent [36].

3.6. Dilatational interfacial rheology of adsorbed supraparticle films

The interfacial films formed during the stabilization of the decane-water emulsion droplets were further studied via dilatational rheology using an oscillating pendant drop setup. This setup allows the direct observation of the dynamic interfacial tension which corresponds to the Gibbs elasticity of the surface. When the droplet surface area is oscillated, the two-dimensional dilatational rheological moduli of the droplet interface can be computed from

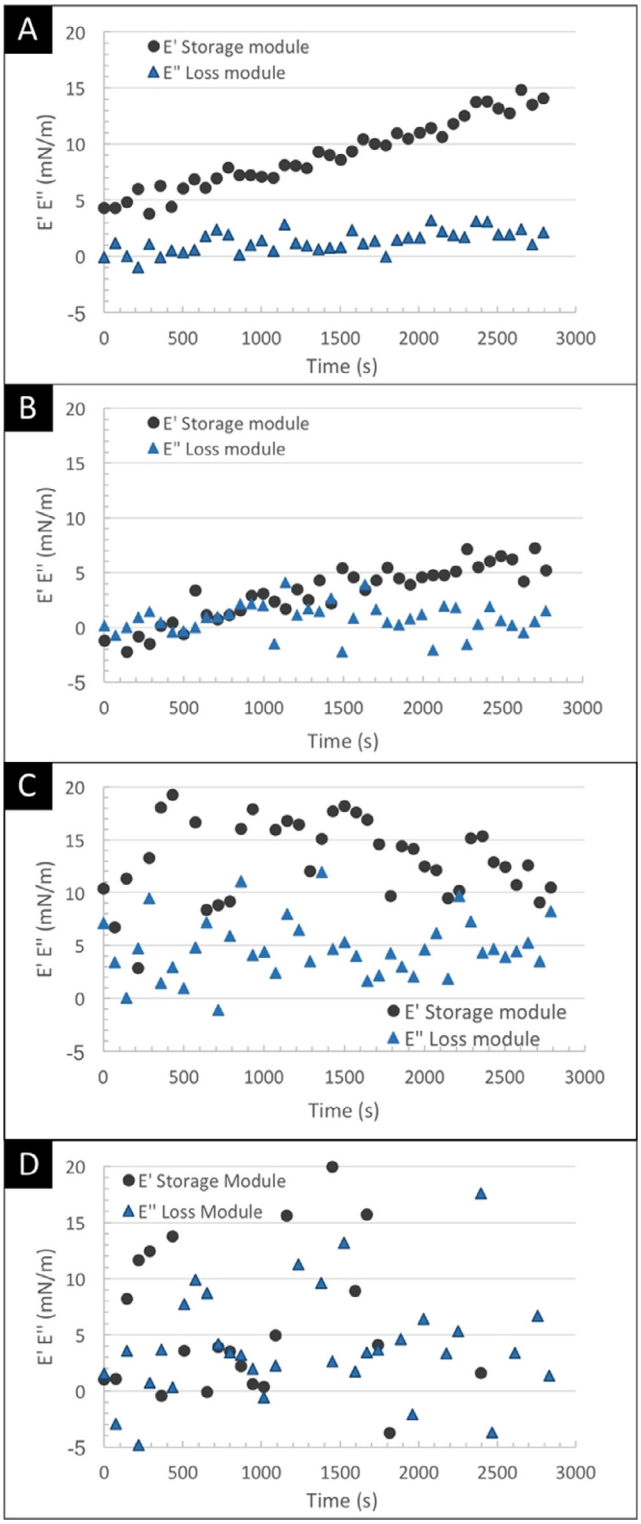

Fig. 8. Interfacial dilatational rheology using the pendant drop method. Time tests with (A) A150+80, (B) A150+OTMS 80, (C) A150 and (D) A150+OTMS.

the frequency and amplitude of the oscillation combined with the phase shift between the surface area oscillations and those of the surface tension of the droplet interface. While, in pendant drop measurements, the interfacial rheological data on the structure of interfacial films is superimposed by dynamic de-and adsorption of surface active components during the measurements (so-called Gibbs-Marangoni effects), the set-up presents a well-established model-system to assess emulsion stability. Our experiments therefore observe changes in the interfacial rheology of water droplets in decane caused by the adsorption of nanoparticles. Since the adsorption of nanoparticles to the interface should be significantly slower than the oscillations of the surface area of the droplet, the resulting graphs mostly represent the formation of nanoparticle films at the droplet interface. In the case of the assembled supraparticles (A150+80), it was possible to observe the growth of a stabilizing interfacial film (Fig. 8a). This further confirms the assumption that the zwitterionic supraparticles are able to form an interlocking, cohesive layer at the droplet interface. Although the amphiphilic supraparticles (A150+80+OTMS) are only able to stabilize emulsions to a lesser extent, the pendant drop results indicate the formation of a cohesive interfacial film, as well (Fig. 8b). However, the complex elastic moduli are smaller than those of the zwitterionic particle film which explains the inferior emulsion stability. All other particles do not show the formation of a cohesive interfacial layer as is indicated by the chaotic results (only shown here for A150 and A150+OTMS, Fig. 8c and d). Here, emulsion stabilization most likely proceeds via the reduction of the interfacial energy as per the above described Pickering law (Eq. (8)).

4. Conclusion

In summary, we investigated the electrostatic assembly of small colloidally stable supraparticles via electrostatic heteroaggregation. Although predicted theoretically [4,5], well-defined and colloidally stable supraparticles on the nanoscale could be realized only in special cases through heteroaggregation [22,23]. In contrast to the expected well-ordered particles, our supraparticles consist of a central APTES-coated silica particle with a diameter of 150 nm and one to six uncoated silica particles with diameters of 80 nm. Furthermore, the particles are adsorbed at seemingly random distances from each other including aggregates of the small particles with each other. Accordingly, instead of producing one type of homogeneous supraparticle, we created a reproducible ensemble of supraparticles that exists as a colloidally stable dispersion. As discussed above, we hypothesize that the aggregation of the small particles can be explained in part by considering the DLVO interactions of the small particles inside the ion cloud of the bigger central particle. In future work, more in depth dynamic Modeling will be explored to substantiate this aspect. Finally, we found that this ensemble of zwitterionic supraparticles is able to stabilize emulsions much more efficiently than the individual particles of the assembly by forming interlocking particle films at the droplet interface. While similar findings have been reported for random agglomerates of positively and negatively charged particles [6,7], our approach allows a well-controlled tailoring of the particle ensemble with a patchy surface structure which can either be zwitterionic or amphiphilic. In this respect, we demonstrated that the relatively unordered ensemble of supraparticles is able to show well-defined functionality at a higher hierarchical level, which hearkens back to the definition of an ensemble in thermodynamics.

Appendix A. Supplementary material

Supplementary data associated with this article can be found, in the online version, at http://dx.doi.org/10.1016/j.jcis.2017.04.076.

References

[1] Y. Wang et al., Colloids with valence and specific directional bonding, Nature 491 (2012) 51–55.
[2] K.J. Stebe, E. Lewandowski, M. Ghosh, Oriented assembly of metamaterials, Science 325 (2009) 159–160.
[3] G.M. Whitesides, The once and future nanomachine, Sci. Am. 285 (2001) 70–75.

[4] M. Cerbelaud et al., Heteroaggregation between Al_2O_3 submicrometer particles and SiO_2 nanoparticles: experiment and simulation, Langmuir 24 (2008) 3001–3008.
[5] M. Cerbelaud et al., Self-assembly of oppositely charged particles in dilute ceramic suspensions: predictive role of simulations, Soft Matter 6 (2010) 370–382.
[6] T. Nallamilli, B.P. Binks, E. Mani, M.G. Basavaraj, Stabilization of Pickering emulsions with oppositely charged latex particles: influence of various parameters and particle arrangement around droplets, Langmuir 31 (2015) 11200–11208.
[7] B.P. Binks, W. Liu, J.A. Rodrigues, Novel stabilization of emulsions via the heteroaggregation of nanoparticles, Langmuir 24 (2008) 4443–4446.
[8] E. Mastrobattista, M.A.E.M. van der Aa, W.E. Hennink, D.J.A. Crommelin, Artificial viruses: a nanotechnological approach to gene delivery, Nat. Rev. Drug Discov. 5 (2006) 115–121.
[9] C.H. Evers, J.A. Luiken, P.G. Bolhuis, W.K. Kegel, Self-assembly of microcapsules via colloidal bond hybridization and anisotropy, Nature (2016).
[10] A.M. Islam, B.Z. Chowdhry, M.J. Snowden, Heteroaggregation in colloidal dispersions, Adv. Coll. Interface. Sci. 62 (1995) 109–136.
[11] Y. Xia et al., Self-assembly of self-limiting monodisperse supraparticles from polydisperse nanoparticles, Nat. Nanotechnol. 6 (2011) 580–587.
[12] M.A. Piechowiak et al., Oppositely charged model ceramic colloids: numerical predictions and experimental observations by confocal laser scanning microscopy, Langmuir 26 (2010) 12540–12547.
[13] S. Rollié, K. Sundmacher, Determination of cluster composition in heteroaggregation of binary particle systems by flow cytometry, Langmuir 24 (2008) 13348–13358.
[14] P.D. Yates, G.V. Franks, G.J. Jameson, Orthokinetic heteroaggregation with nanoparticles: effect of particle size ratio on aggregate properties, Colloids Surf. Physicochem. Eng. Aspects 326 (2008) 83–91.
[15] J.M. López-López, A. Schmitt, A. Moncho-Jordá, R. Hidalgo-Álvarez, Electrostatic heteroaggregation regimes in colloidal suspensions, Adv. Coll. Interface. Sci. 147–148 (2009) 186–204.
[16] S.L. Westcott, S.J. Oldenburg, T.R. Lee, N.J. Halas, Formation and adsorption of clusters of gold nanoparticles onto functionalized silica nanoparticle surfaces, Langmuir 14 (1998) 5396–5401.
[17] A.F. Demirörs et al., Long-ranged oppositely charged interactions for designing new types of colloidal clusters, Phys. Rev. X 5 (2015) 021012.
[18] J.N. Israelachvili, Intermolecular and Surface Forces: Revised, third ed., Academic Press, 2011.
[19] G.M. Torrie, J.P. Valleau, Electrical double layers. I. Monte Carlo study of a uniformly charged surface, J. Chem. Phys. 73 (1980) 5807–5816.
[20] Wiley: Physics and Chemistry of Interfaces – Hans-Jürgen Butt, Karlheinz Graf, Michael Kappl. Available at: <http://eu.wiley.com/WileyCDA/WileyTitle/productCd-3527606408.html> (accessed: 19th October 2016).
[21] S. Bhattacharjee, M. Elimelech, M. Borkovec, DLVO interaction between colloidal particles: beyond Derjaguin's approximation, Croat. Chem. Acta 71 (1998) 883–903.
[22] P. Dušak, A. Mertelj, S. Kralj, D. Makovec, Controlled heteroaggregation of two types of nanoparticles in an aqueous suspension, J. Colloid Interface Sci. 438 (2015) 235–243.
[23] C.S. Wagner, S. Shehata, K. Henzler, J. Yuan, A. Wittemann, Towards nanoscale composite particles of dual complexity, J. Colloid Interface Sci. 355 (2011) 115–123.
[24] E.W. Edwards, D. Wang, H. Möhwald, Hierarchical organization of colloidal particles: from colloidal crystallization to supraparticle chemistry, Macromol. Chem. Phys. 208 (2007) 439–445.
[25] J. Du, R.K. O'Reilly, Anisotropic particles with patchy, multicompartment and Janus architectures: preparation and application, Chem. Soc. Rev. 40 (2011) 2402–2416.
[26] G.-R. Yi, D.J. Pine, S. Sacanna, Recent progress on patchy colloids and their self-assembly, J. Phys.: Condens. Matter 25 (2013) 193101.
[27] G. Loglio et al., Drop and bubble shape analysis as a tool for dilational rheological studies of interfacial layers, Stud. Interface Sci. 11 (2001) 439–483.
[28] C. Kloss, C. Goniva, A. Hager, S. Amberger, S. Pirker, Models, algorithms and validation for opensource DEM and CFD–DEM, Prog. Comput. Fluid Dyn. Int. J. 12 (2012) 140–152.
[29] W. Lin et al., Heteroaggregation in binary mixtures of oppositely charged colloidal particles, Langmuir 22 (2006) 1038–1047.
[30] Y. Zhang, Y. Chen, P. Westerhoff, K. Hristovski, J.C. Crittenden, Stability of commercial metal oxide nanoparticles in water, Water Res. 42 (2008) 2204–2212.
[31] Q. Li, U. Jonas, X.S. Zhao, M. Kappl, The forces at work in colloidal self-assembly: a review on fundamental interactions between colloidal particles, Asia-Pac. J. Chem. Eng. 3 (2008) 255–268.
[32] J. Laube, S. Salameh, M. Kappl, L. Mädler, L. Colombi Ciacchi, Contact forces between TiO_2 nanoparticles governed by an interplay of adsorbed water layers and roughness, Langmuir 31 (2015) 11288–11295.
[33] S. Salameh et al., Adhesion mechanisms of the contact interface of TiO_2 nanoparticles in films and aggregates, Langmuir 28 (2012) 11457–11464.
[34] A. Fabre, S. Salameh, L.C. Ciacchi, M.T. Kreutzer, J.R. van Ommen, Contact mechanics of highly porous oxide nanoparticle agglomerates, J. Nanopart. Res. 18 (2016) 1–13.
[35] T. Bollhorst et al., Bifunctional submicron colloidosomes coassembled from fluorescent and superparamagnetic nanoparticles, Angew. Chem. 127 (2015) 120–125.
[36] B.P. Binks, S.O. Lumsdon, Pickering emulsions stabilized by monodisperse latex particles: effects of particle size, Langmuir 17 (2001) 4540–4547.